Research Square

Preprints are preliminary reports that have not undergone peer review.
They should not be considered conclusive, used to inform clinical practice,
or referenced by the media as validated information.

Performance Analysis of Integrated Satellite-Aerial IoT Networks for Remote Environmental Monitoring With Link Switching Scheme

Xinyue He
Nanjing University of Aeronautics and Astronautics
Kefeng Guo
Kefeng_Guo@nuaa.edu.cn
Nanjing University of Aeronautics and Astronautics
Jiajing Wu
Nanjing University of Aeronautics and Astronautics
Ali Nauman
Yeungnam University
Caicheng Tong
Nanjing University of Aeronautics and Astronautics
Caitong Chen
Nanjing University of Aeronautics and Astronautics
Qihui Wu
Nanjing University of Aeronautics and Astronautics
Yazeed Alsarhan
Hourani Center for Applied Scientific Research, Al-Ahliyya Amman University

Research Article

Keywords: Integrated satellite-aerial IoT network, link switching scheme, optimization method, performance analysis

Posted Date: October 30th, 2026

DOI: https://doi.org/10.21203/rs.3.rs-11146859/v1

License: This work is licensed under a Creative Commons Attribution 4.0 International License.
Read Full License

Additional Declarations: No competing interests reported.

Performance Analysis of Integrated Satellite-Aerial IoT Networks for Remote Environmental Monitoring With Link Switching Scheme

Xinyue He[1], Kefeng Guo[1*], Jiajing Wu[1], Ali Nauman[2], Caicheng Tong[1], Caitong Chen[1], Qihui Wu[1], Yazeed Alsarhan[3]

[1] College of Electronic and Information Engineering, Nanjing University of Aeronautics and Astronautics, Nanjing, 211106, China .

[2] School of Computer Science and Engineering, Yeungnam University, Gyeongsan, 38541, Republic of Korea .

[3] Department of Computer Science, Hourani Center for Applied Scientific Research, Al-Ahliyya Amman University, Amman, Jordan .

*Corresponding author(s). E-mail(s): Kefeng_Guo@nuaa.edu.cn;
Contributing authors: hehedy313@gmail.com; jiajing-wu@nuaa.edu.cn; anauman@ynu.ac.kr; 2326717798@qq.com; 2230363098@qq.com; wuqihui@nuaa.edu.cn; y.alsarhan@ammanu.edu.jo;

Abstract

In remote environmental monitoring Internet of Things (IoT) deployments, UAV-ground direct links frequently experience hard blockage, whereas satellite relay transmission requires higher power. Therefore, an effective link-switching mechanism is needed to balance communication reliability and UAV energy consumption. To address these challenges, an integrated satellite-aerial IoT system is considered for remote environmental monitoring. Sensor data are aggregated by an unmanned aerial vehicle (UAV) and transmitted through either a short-range direct link with Rician fading or a two-hop satellite relay path with Shadowed-Rician fading. Specifically, a new link switching scheme is proposed. The ground terminal uses the low-power direct link by default and activates the satellite relay only upon hard blockage or when the signal-to-noise ratio falls below a switching threshold. Based on the proposed scheme, outage probability, ergodic capacity,

and average bit error rate are derived in closed-form for the considered system. Numerical results verify that the shadowing parameter, blockage probability, and the proposed switching strategy significantly affect the overall system performance. The proposed strategy yields 87%–99% outage reduction across three monitoring scenarios, and the relay activation frequency is primarily governed by the blockage probability rather than shadowing conditions.

Keywords: Integrated satellite-aerial IoT network, link switching scheme, optimization method, performance analysis

1 Introduction

It is well known that satellites can provide wide-area coverage within their service footprints. This inherent characteristic makes satellite communications (SatComs) particularly attractive in remote areas, where wired or wireless terrestrial networks are difficult or impractical to deploy [1, 2]. In addition to fixed satellite services, SatCom also supports mobile satellite services. Many land mobile SatCom systems, such as Inmarsat, Globalstar, and Iridium, have already operated in L or S bands to provide various services, such as voice, data, and image communications for users all over the world. Furthermore, in critical or emergency situations where terrestrial communication infrastructure is damaged or unavailable, satellite systems can provide reliable communication connectivity [1].

With the rapid development of unmanned aerial vehicle (UAV) technology, UAVs have become useful aerial sensing platforms for environmental monitoring [3]. They benefit from flexible deployment, hovering observation capability, and high-resolution imaging. Integrating UAVs into satellite Internet of Things (IoT) enables wide-area backhaul of aerial inspection data, thereby constructing an integrated air-space-ground monitoring system. However, the two available transmission modes exhibit complementary but distinct characteristics. The short-range UAV-to-ground direct link can provide favorable communication performance under LoS conditions. Vegetation can introduce additional penetration loss in UAV-to-ground communications [4]. In this

paper, severe terrain or vegetation obstruction is modeled as a hard-blockage event. In contrast, the satellite relay link provides extensive coverage independent of terrestrial infrastructure, while it is constrained by shadow fading and propagation losses, resulting in lower reliability and higher required transmit power compared with the direct link. Consequently, how to efficiently exploit the complementary characteristics of these two heterogeneous links constitutes a critical open research issue for UAV-based environmental monitoring systems supported by satellite-IoT.

1.1 Background and Motivation

Despite its many advantages, SatCom is more challenging than terrestrial communication, mainly due to the complexity of satellite channels. For land mobile SatComs, random shadowing over satellite-terrestrial links is commonly characterized by the Shadowed-Rician (SR) distribution [5]. This model incorporates Rician-dominated LoS components, whose amplitude fluctuations are modeled by the Nakagami-m distribution. The SR model has been shown to provide a mathematically tractable representation consistent with measured land-mobile satellite channel statistics [5].

Based on the SR channel model, the performance of mobile SatCom systems has been analytically studied in [6–8]. However, these works do not consider the coexistence of heterogeneous direct and satellite-relay links with link switching. In practical scenarios, obstacles and shadowing often degrade satellite-ground line-of-sight (LoS) connectivity. Related hybrid satellite-terrestrial relay architectures have been investigated under different network topologies and channel models [9–11]. For example, [9] considers a maritime IoT architecture involving LEO satellites and UAVs, [10] studies LEO–HAPS–BS relaying, and [11] analyzes overlay spectrum sharing with secondary-network selection in a hybrid satellite-terrestrial system.

In practice, the satellite is often used as a space relay node, which assists signal transmission between the source earth station and the destination. For example,

by assuming that both the uplink and downlink experience SR fading, Bhatnagar [6] analyzed the performance of a dual-hop decode-and-forward (DF) satellite relay system. More recently, satellite relay systems have been investigated from different performance and energy-related perspectives. Bhatnagar [6] analyzed the BER, outage probability, and diversity performance of dual-hop DF satellite relaying, while [12] investigated outage and throughput performance in a battery-aided SWIPT space-air-ground integrated network.

The emergence of UAVs brings new possibilities for remote monitoring applications. Under LoS-dominant conditions, UAV-to-ground short-range links are commonly modeled using Rician fading [3, 13]. Although such direct links can achieve high data rates under favorable propagation conditions, they remain vulnerable to hard blockage caused by terrain occlusion and vegetation shielding. In this context, recent advances have promoted the development of integrated satellite-aerial IoT networks, where UAVs serve as aerial nodes cooperate with satellite connectivity to support wide-area IoT services [14, 15]. Related studies have investigated NOMA-based satellite-UAV networking [16], RIS-assisted wireless transmission [17], spectrum sharing and relay selection in hybrid satellite-terrestrial networks [18], and UAV trajectory optimization in satellite-UAV IoT systems [19]. Although fruitful results have been achieved, these studies address transmission and optimization mechanisms different from the direct-link-priority primary-backup architecture considered in this work.

Link and relay selection mechanisms have been investigated in hybrid satellite-terrestrial networks [11, 20]. These studies consider network architectures and selection objectives different from the direct-link-priority primary-backup scheme adopted here. In this work, hard blockage of the UAV-ground direct link is explicitly incorporated into the switching rule. This factor is particularly critical for remote environmental-monitoring scenarios, where terrain occlusion and vegetation shielding

often break LoS connectivity. Furthermore, few prior works combine the integrated satellite-aerial IoT network architecture with link-switching optimization. In particular, few existing frameworks are customized for remote environmental-monitoring deployments, where shadowing severity and blockage probability vary drastically across different field scenarios.

To the best of our knowledge, limited prior work has jointly considered hard blockage and shadow fading in UAV-based satellite-aerial IoT systems with primary-backup link switching over heterogeneous Rician/SR channels.

1.2 Our Contributions

Motivated by the aforementioned observations, this paper investigates the performance of a UAV-based environmental monitoring system supported by satellite-IoT. An air-space-ground hybrid link model under SR heterogeneous channels is established, together with a primary-backup switching strategy incorporating an optimized threshold and power allocation. The main contributions of this work are summarized as follows.

- A hybrid system model is established in an integrated satellite-aerial IoT network for remote environmental monitoring. Unlike existing studies of integrated satellite-aerial networks that evaluate only a single transmission path, the developed model jointly accounts for the Rician-faded direct link, the two-hop DF satellite relay link with SR fading, and the hard-blockage effect on the direct link. A primary-backup switching mechanism is enabled to adapt to practical environmental monitoring scenarios.
- A primary-backup link switching scheme with joint threshold optimization and power allocation is proposed. Strict opposite monotonicity between system outage probability and average UAV transmit power with respect to the switching threshold is proven. This property reduces the constrained power-minimization problem into

a one-dimensional root-finding problem. Different from previous HSTRN research concentrating on ground multi-relay selection, the proposed scheme works between the UAV-ground direct link and the satellite relay backup. Hard blockage is explicitly used as a switching trigger. The parameter region with a strictly positive optimal threshold is also characterized to identify the conditions under which SNR-triggered switching is required in addition to blockage-triggered switching.

- Analytical expressions for outage probability, ergodic capacity and average bit error rate (BER) are derived for individual transmission paths as well as the proposed switching system. Asymptotic analysis in the high signal-to-noise ratio (SNR) regime is conducted to uncover the diversity order and coding gain. Monte Carlo simulations are conducted to verify the theoretical derivations and investigate the effects of key system parameters.

The rest of this paper is organized as follows. Section 2 introduces the system model followed by the channel and signal formulations. Section 3 investigates the statistical characteristics of the fading channels and derives the analytical performance expressions for the three transmission paths, including outage probability, ergodic capacity, and average BER. In Section 4, the link switching strategy and power allocation optimization scheme are proposed. In Section 5, Monte Carlo simulation results are provided to validate the analytical results and to discuss the impacts of key system parameters. Finally, Section 6 concludes this paper.

1.3 Notations

$f_X(\cdot)$ and $F_X(\cdot)$ denote the probability density function (PDF) and cumulative distribution function (CDF) of the random variable X, respectively. $\bar{\gamma}$ denotes the average SNR. $I_0(\cdot)$ denotes the zeroth-order modified Bessel function of the first kind. ${}_1F_1(\cdot;\cdot;\cdot)$ denotes the confluent hypergeometric function of the first kind (Kummer's function). $\mathrm{erfc}(\cdot)$ denotes the complementary error function. $\min(\cdot,\cdot)$ and $\max(\cdot,\cdot)$ denote the

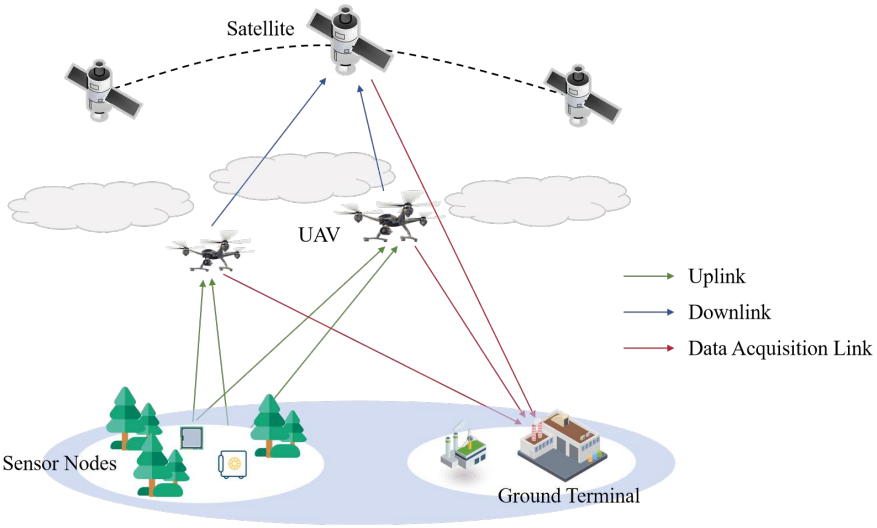


Fig. 1 Architecture of the Space-Air-Ground Hybrid IoT System

minimum and maximum operations, respectively. $\mathbb{E}[\cdot]$ denotes the expectation operator. $\mathcal{CN}(\cdot,\cdot)$ denotes the complex Gaussian distribution. $\|\cdot\|$ denotes the Euclidean norm of a vector.

2 System Model and Problem Formulation

As illustrated in Fig. 1, this paper considers a UAV-based environmental monitoring system assisted by satellite IoT, where a low-altitude UAV acts as the aerial sensing node for data backhaul. Two heterogeneous transmission paths are utilized, including a UAV-ground direct link and a two-hop UAV-satellite-ground DF relay link. The direct link provides high-rate, low-latency transmission but suffers from terrain and vegetation-induced hard blockage, while the satellite relay link guarantees broad coverage but is affected by shadow fading and propagation attenuation. Considering the stationary feature of geostationary satellites, the Doppler effect is neglected in channel modeling. This paper incorporates the direct-link hard-blockage characteristic and optimizes the path-switching threshold to minimize UAV power consumption under

outage constraints. The satellite downlink power is fixed and not included in the UAV power optimization.

2.1 Channel Modeling

The considered hybrid air-space-ground system comprises two heterogeneous wireless links: the low-altitude UAV-ground direct link and the satellite two-hop relay link. These channels exhibit distinct fading characteristics due to different propagation environments. In this subsection, the statistical channel models for both transmission paths are formulated.

2.1.1 Low-Altitude Direct Link: Rician Fading

Due to the low flight altitude of the UAV, the direct UAV-ground channel is dominated by a strong LoS component, which can be accurately modeled using Rician fading. The instantaneous SNR γ_d of the direct link follows a Rician distribution with the PDF expressed as

$$f_{\gamma_d}(\gamma) = \frac{1+K_d}{\bar{\gamma}_d} \exp\left(-K_d - \frac{(1+K_d)\gamma}{\bar{\gamma}_d}\right) I_0\left(2\sqrt{\frac{K_d(1+K_d)\gamma}{\bar{\gamma}_d}}\right), \quad \gamma \geq 0, \quad (1)$$

where $\bar{\gamma}_d$ denotes the average SNR of the direct link, K_d is the Rician K-factor representing the power ratio between the LoS path and scattered multipath components, and $I_0(\cdot)$ is the zeroth-order modified Bessel function of the first kind.

2.1.2 Satellite Link: SR Fading

Different from terrestrial direct channels, satellite propagation suffers from both multipath fading and random shadowing caused by atmospheric occlusion and ground clutter. The SR model is adopted herein to characterize satellite uplink and downlink

channels. Let γ_s denote the instantaneous SNR of the satellite link. Its PDF is given by

$$f_{\gamma_s}(x) = \frac{1+K_s}{\bar{\gamma}_s}\left(\frac{m}{m+K_s}\right)^m \exp\left(-\frac{(1+K_s)x}{\bar{\gamma}_s}\right), \\ \times {}_1F_1\left(m;\, 1;\, \frac{K_s(1+K_s)x}{(m+K_s)\bar{\gamma}_s}\right), \quad x \geq 0, \tag{2}$$

where $\bar{\gamma}_s$ is the average satellite-link SNR, K_s denotes the satellite Rician K-factor, and m represents the shadowing severity parameter. The shadowing degree increases with decreasing m. Particularly, the SR model degenerates to the standard Rician fading model when $m \to \infty$.

2.1.3 Equivalent SNR of Two-Hop DF Relay Link

For the DF satellite relay transmission, the overall communication success relies on both the UAV-satellite uplink and satellite-ground downlink. Let γ_u and γ_v denote the instantaneous SNRs of the uplink and downlink, respectively. According to the DF protocol, the end-to-end transmission quality is determined by the weaker hop. Therefore, the equivalent SNR of the two-hop relay link is formulated as

$$\gamma_r = \min(\gamma_u, \gamma_v). \tag{3}$$

Accordingly, the outage event occurs if either hop fails to satisfy the quality-of-service requirement. The overall outage probability of the relay path can be further derived based on the statistical characteristics of γ_u and γ_v.

2.2 Signal Model

Two transmission modes are adopted in the hybrid system. Under normal conditions, the UAV sends aggregated sensor data directly to the ground terminal. The received signal at the ground terminal is expressed as

$$y_d = \sqrt{P_d} h_d s + n_d, \tag{4}$$

where P_d denotes the transmit power of the direct link, h_d is the Rician fading channel coefficient, s denotes the unit-power transmitted symbol satisfying $\mathbb{E}[|s|^2] = 1$, and n_d represents the additive white Gaussian noise (AWGN) with variance σ_d^2.

Once hard blockage occurs or the instantaneous SNR of the direct link drops below the switching threshold, the UAV switches to the satellite relay path. The signal received by the GEO satellite through the UAV uplink is

$$y_u = \sqrt{P_s} h_u s + n_u, \tag{5}$$

where P_s is the UAV uplink transmit power for satellite relay. After decoding, the satellite re-encodes and forwards the signal to the ground terminal over the downlink:

$$y_v = \sqrt{P_v} h_v s + n_v, \tag{6}$$

where P_v is the fixed onboard satellite downlink transmit power. h_u, h_v are Shadowed-Rician channel coefficients for the uplink and downlink, respectively. n_u and n_v denote AWGN with variance σ_u^2 and σ_v^2.

For the DF relay protocol, successful end-to-end delivery requires correct decoding on both uplink and downlink hops, and any hop failure leads to relay transmission outage. Note that the ground terminal does not perform signal combining. Only one path is activated at a time following the switching strategy presented in Section 4. Perfect channel state information (CSI) is assumed available at the ground terminal for link-switching decisions, which is a widely used assumption in related literature. In addition, the sensor-to-UAV data acquisition link is assumed to be fully reliable and is beyond the scope of this work.

3 Performance Analysis

Based on the system model established in Section 2, this section derives the analytical expressions for the outage probability, ergodic capacity, and average BER

under quadrature phase-shift keying (QPSK) modulation for the three transmission paths. The impact of average SNR, satellite shadowing parameter, elevation angle, and direct-link hard-blockage probability on system performance is also discussed.

3.1 Statistical Characteristics of the Equivalent SNR

3.1.1 Direct Link: Rician PDF and CDF

The instantaneous SNR γ_d of the UAV-to-ground direct link follows a Rician distribution. Its PDF is provided in (1), and the corresponding CDF is derived via integral calculation as

$$F_{\gamma_d}(\gamma) = 1 - Q_1\left(\sqrt{2K_d}, \sqrt{\frac{2(1+K_d)\gamma}{\bar{\gamma}_d}}\right), \tag{7}$$

where $Q_1(\cdot,\cdot)$ denotes the first-order Marcum Q-function. Under typical low-altitude UAV communication configurations with $K_d = 10$ dB, the LoS component dominates multipath scattering. The outage probability characterized by $F_{\gamma_d}(\gamma_{\text{svc}})$ decays rapidly as the average SNR $\bar{\gamma}_d$ increases.

3.1.2 Satellite Links: SR PDF and CDF

For both satellite uplink and downlink hops, the instantaneous SNR γ_s follows the SR fading distribution, whose PDF is given in (2). By integrating the PDF over $[0, \gamma]$, the CDF is expressed as

$$F_{\gamma_s}(\gamma) = 1 - \alpha_s \sum_{k=0}^{m-1} \frac{\zeta(k)}{\bar{\gamma}_s^k} \sum_{t=0}^{k} \frac{k!}{t!} \Delta_s^{-(k+1-t)} \gamma^t e^{-\Delta_s \gamma}, \tag{8}$$

where $\alpha_s = \left(\frac{2b_s m}{2b_s m + \Omega_s}\right)^m / 2b_s$, $\zeta(k) = \frac{(-1)^k (1-m)_k \delta_s^k}{(k!)^2}$, and $\Delta_s = \frac{1/(2b_s) - \delta_s}{\bar{\gamma}_s}$. Specifically, Ω_s and $2b_s$ represent the average power of the LoS and multipath components of satellite channels, respectively, and $\delta_s = \frac{\Omega_s}{2b_s(2b_s m + \Omega_s)}$.

The shadowing parameter m characterizes the fading severity of satellite links. A smaller m corresponds to more severe shadowing attenuation. In particular, the SR model degenerates to the standard Rician distribution as $m \to \infty$.

3.1.3 Two-Hop DF Relay: Equivalent SNR CDF and PDF

For the two-hop DF relay transmission, the end-to-end quality is governed by the weaker hop, yielding $\gamma_r = \min(\gamma_u, \gamma_v)$. Let $F_u(\cdot)$ and $F_v(\cdot)$ denote the CDFs of the uplink and downlink SNRs, respectively. Similarly, $f_u(\cdot)$ and $f_v(\cdot)$ represent the corresponding PDFs, where both SNR sequences follow the Shadowed-Rician (SR) model given in (2). The CDF of γ_r is derived as

$$F_r(\gamma) = 1 - \big(1 - F_u(\gamma)\big)\big(1 - F_v(\gamma)\big). \tag{9}$$

Differentiating (9) yields the PDF of the equivalent relay SNR:

$$f_r(\gamma) = f_u(\gamma)\big(1 - F_v(\gamma)\big) + f_v(\gamma)\big(1 - F_u(\gamma)\big). \tag{10}$$

The above statistical expressions provide the mathematical basis for the outage probability, ergodic capacity, and bit error rate analysis of the hybrid relay system in the subsequent sections.

3.2 Performance of the Three Transmission Paths

Based on the statistical characteristics derived in Section 3, this subsection provides analytical performance expressions for three transmission schemes, including practical direct transmission, practical DF relay transmission, and ideal selection combining (SC) benchmark. The first two schemes characterize the actual hybrid transmission modes of the considered system, while the ideal SC scheme is introduced as a performance upper bound. Specifically, the SC strategy assumes full instantaneous CSI of both links and always selects the superior channel, which is impractical because of hardware constraints and is used only as a theoretical benchmark.

3.2.1 Performance of the Direct Path

The outage probability is defined as the probability that the instantaneous SNR falls below the predefined service threshold γ_{svc}. Substituting the Rician CDF derived in (7), the outage probability of the direct link is written as

$$P_{\mathrm{out},d} = F_{\gamma_d}(\gamma_{\mathrm{svc}}) = 1 - Q_1\left(\sqrt{2K_d}, \sqrt{\frac{2(1+K_d)\gamma_{\mathrm{svc}}}{\bar{\gamma}_d}}\right). \tag{11}$$

The ergodic capacity and average QPSK bit error rate are obtained by averaging the instantaneous performance over the Rician fading distribution:

$$C_d = \int_0^\infty \log_2(1+\gamma) f_{\gamma_d}(\gamma)\, d\gamma, \tag{12}$$

$$P_{b,d} = \int_0^\infty \frac{1}{2}\,\mathrm{erfc}\left(\sqrt{\gamma}\right) f_{\gamma_d}(\gamma)\, d\gamma, \tag{13}$$

where $f_{\gamma_d}(\gamma)$ denotes the Rician PDF given in (1). With $K_d = 10$ dB, the LoS component is dominant, and the performance of the direct link improves rapidly as the average SNR increases.

3.2.2 Performance of the Two-Hop DF Relay Path

For the two-hop DF relay link, the end-to-end equivalent SNR follows $\gamma_r = \min(\gamma_u, \gamma_v)$, whose CDF and PDF are derived in (9) and (10), respectively. Accordingly, the outage probability of the relay path is given by

$$P_{\mathrm{out},r} = F_r(\gamma_{\mathrm{svc}}) = 1 - \big(1 - F_u(\gamma_{\mathrm{svc}})\big)\big(1 - F_v(\gamma_{\mathrm{svc}})\big). \tag{14}$$

It can be observed that the relay transmission is in outage if either the uplink or downlink transmission fails, which is consistent with the inherent characteristics of the DF relay protocol.

Considering the half-duplex constraint of practical satellite relay systems, two orthogonal time slots are required for one complete two-hop transmission. Therefore,

the ergodic capacity is expressed as

$$C_r = \frac{1}{2} \int_0^\infty \log_2(1+\gamma) f_r(\gamma)\, d\gamma. \tag{15}$$

Similarly, the average BER of the relay path is approximated by the equivalent-SNR approach, which treats the two-hop DF link as a single link with instantaneous SNR equal to the minimum of the two hops. The expression is given by

$$P_{b,r} \approx \int_0^\infty \frac{1}{2} \operatorname{erfc}\left(\sqrt{\gamma}\right) f_r(\gamma)\, d\gamma. \tag{16}$$

This approximation is widely adopted in the literature for its analytical tractability and becomes increasingly accurate at high SNR where the bottleneck hop dominates the error performance. A more precise treatment would involve the two-hop error propagation formula $P_{b,r} = P_{b,u} + P_{b,v} - 2P_{b,u}P_{b,v}$, where $P_{b,u}$ and $P_{b,v}$ are the per-hop BERs. Owing to the bottleneck effect inherent in two-hop transmission, the relay path generally exhibits a higher outage probability and BER than the direct link under identical average SNR conditions.

3.2.3 Performance of Ideal Selection Combining (Benchmark)

To quantitatively evaluate the performance gain of the proposed hybrid switching scheme, an ideal SC benchmark is adopted. The ideal SC strategy selects the maximum instantaneous SNR from the two independent paths, i.e., $\gamma_{\mathrm{SC}} = \max(\gamma_d, \gamma_r)$. The system outage occurs only when both paths are in outage simultaneously, yielding

$$P_{\mathrm{out,SC}} = P_{\mathrm{out},d} \cdot P_{\mathrm{out},r}. \tag{17}$$

The corresponding PDF of the maximum-combined SNR is given by

$$f_{\mathrm{SC}}(\gamma) = f_d(\gamma)F_r(\gamma) + f_r(\gamma)F_d(\gamma). \tag{18}$$

Based on the derived PDF, the ergodic capacity and average BER of the SC benchmark are expressed as

$$C_{\mathrm{SC}} = \int_0^\infty \log_2(1+\gamma) f_{\mathrm{SC}}(\gamma)\, d\gamma, \tag{19}$$

$$P_{b,\mathrm{SC}} = \int_0^\infty \frac{1}{2}\,\mathrm{erfc}\left(\sqrt{\gamma}\right) f_{\mathrm{SC}}(\gamma)\, d\gamma. \tag{20}$$

Ideal SC provides the best performance in terms of outage probability and BER, and therefore serves as the theoretical upper bound of the hybrid system. Nevertheless, it requires real-time full-CSI acquisition of both links and parallel signal reception, which is impractical for energy-constrained UAV IoT scenarios.

3.3 Asymptotic Performance Analysis

To reveal the fundamental performance limits and key parameter impacts in high-SNR scenarios, this subsection conducts asymptotic outage analysis for the considered hybrid system. The diversity order and coding gain are also analyzed to provide engineering insights.

3.3.1 Asymptotic Outage Probability

In the high-SNR regime where the average SNR approaches infinity, the system performance is governed by the low-order fading term. Accordingly, the CDFs of fading channels can be simplified via first-order asymptotic approximation.

For the Rician fading-based direct link, the asymptotic CDF is given by

$$F_{\gamma_d}^{\infty}(\gamma) \simeq \frac{(1+K_d)e^{-K_d}}{\bar{\gamma}_d}\gamma + o\left(\frac{1}{\bar{\gamma}_d}\right), \tag{21}$$

where the factor e^{-K_d} arises from the first-order series expansion of the modified Bessel function $I_0(\cdot)$ in the Rician PDF (1) at high SNR. For $K_d = 10$ dB, this factor equals approximately 4.5×10^{-5}, indicating that the LoS dominance significantly reduces the coding gain of the direct link.

For each SR satellite hop, the asymptotic CDF is approximated as

$$F_{\gamma_s}^{\infty}(\gamma) \simeq \frac{\alpha_s}{\bar{\gamma}_s}\gamma + o\left(\frac{1}{\bar{\gamma}_s}\right), \tag{22}$$

where α_s is the channel coefficient defined in (8).

Substituting the asymptotic CDF into the outage definition, the high-SNR outage probability of the direct path is derived as

$$P_{\text{out},d}^{\infty} \simeq \frac{(1+K_d)e^{-K_d}}{\bar{\gamma}_d}\gamma_{\text{svc}}. \tag{23}$$

For the two-hop DF relay path, the end-to-end outage probability is determined by the superposition of the first-order asymptotic terms of two independent hops. Substituting the statistical property of $\gamma_r = \min(\gamma_u, \gamma_v)$, the asymptotic relay outage is expressed as

$$P_{\text{out},r}^{\infty} \simeq \left(\frac{\alpha_u}{\bar{\gamma}_u} + \frac{\alpha_v}{\bar{\gamma}_v}\right)\gamma_{\text{svc}}, \tag{24}$$

where α_u and α_v denote the SR coefficients for satellite uplink and downlink, respectively.

3.3.2 Diversity Order and Coding Gain Analysis

Diversity order characterizes the decay slope of outage probability in the high-SNR region, which is formally defined as

$$G_d = -\lim_{\bar{\gamma}\to\infty} \frac{\log P_{\text{out}}(\bar{\gamma})}{\log \bar{\gamma}}. \tag{25}$$

From (23) and (24), both the direct link and the two-hop relay link achieve a diversity order of $G_d = 1$. Different from the individual paths, the ideal SC benchmark satisfies $P_{\text{out,SC}}^{\infty} \propto \bar{\gamma}^{-2}$, yielding a higher diversity order of $G_d = 2$.

It is noteworthy that the system parameters mainly affect the coding gain rather than the diversity order. Specifically, the Rician K-factor and satellite shadowing

parameter m jointly determine the coding gain of the individual paths. Severe shadowing (smaller m) degrades the relay path reliability by reducing the coding gain, while the outage decay slope remains unchanged. It should be noted that the direct-link hard-blockage probability q does not appear in the asymptotic expressions of the individual paths, as it characterizes the link-switching behavior rather than the fading statistics. The asymptotic performance of the complete switching system, which incorporates the effect of q, is governed by the switching threshold γ_{th}^{*} and is discussed in Section 4. This demonstrates that improving satellite channel conditions can effectively reduce the relay outage floor, while the blockage probability influences the switching frequency and the overall system outage through the link-selection mechanism.

4 Switching Strategy and Power Allocation Optimization

4.1 System Average Power Consumption Model

The ground terminal adopts a primary/backup switching strategy: it defaults to the low-power UAV-to-ground direct link and switches to the satellite relay path only when the direct link is in hard blockage or its instantaneous SNR falls below a preset switching threshold γ_{th}. Let $q \in (0,1)$ denote the hard-blockage probability of the direct link. The transmit powers of the direct link and the satellite uplink are denoted by P_d and P_s, respectively. The satellite downlink power P_v is a fixed onboard resource and is not included in the UAV-side power budget.

For a given switching threshold γ_{th}, the probability that the system selects the direct path is

$$p_d(\gamma_{\mathrm{th}}) = (1-q)\big[1 - F_d(\gamma_{\mathrm{th}})\big], \tag{26}$$

and the probability of selecting the satellite relay path is

$$p_r(\gamma_{\text{th}}) = q + (1-q)F_d(\gamma_{\text{th}}), \tag{27}$$

where $F_d(\cdot)$ is the CDF of the Rician fading channel for the direct link, as derived in (7). The average power consumption of the UAV is then given by

$$P_{\text{avg}}(\gamma_{\text{th}}) = p_d(\gamma_{\text{th}})P_d + p_r(\gamma_{\text{th}})P_s. \tag{28}$$

Since the satellite link has a much longer transmission distance than the direct link, typically $P_s > P_d$, frequent switching to the satellite relay increases the average power consumption of the UAV.

4.2 Optimal Switching Threshold Design

4.2.1 Problem Formulation

Under the primary/backup switching strategy, the system outage probability consists of two components: (i) the direct path is selected but its instantaneous SNR falls below the service threshold γ_{svc}; (ii) the relay path is selected but the relay transmission fails. The outage probability is thus expressed as

$$P_{\text{out}}(\gamma_{\text{th}}) = (1-q)\big[F_d(\gamma_{\text{svc}}) - F_d(\gamma_{\text{th}})\big] + \big[q + (1-q)F_d(\gamma_{\text{th}})\big]P_{\text{out},r}, \tag{29}$$

where $F_d(\gamma_{\text{svc}}) = P_{\text{out},d}$ is the outage probability of the direct link, and $P_{\text{out},r}$ is the outage probability of the relay path given in (14).

The optimal switching threshold problem is formulated as

$$\min_{\gamma_{\text{th}}} \; P_{\text{avg}}(\gamma_{\text{th}}) \quad \text{s.t.} \quad P_{\text{out}}(\gamma_{\text{th}}) \le \epsilon_{\text{th}}, \quad 0 \le \gamma_{\text{th}} \le \gamma_{\text{svc}}, \tag{30}$$

where ϵ_{th} is the maximum tolerable outage probability.

4.2.2 Solution via Monotonicity Analysis

Taking the derivative of $P_{\text{out}}(\gamma_{\text{th}})$ in (29) with respect to γ_{th} yields

$$\frac{\partial P_{\text{out}}}{\partial \gamma_{\text{th}}} = -(1-q) f_d(\gamma_{\text{th}})(1 - P_{\text{out},r}) < 0, \tag{31}$$

which indicates that $P_{\text{out}}(\gamma_{\text{th}})$ is monotonically decreasing with respect to γ_{th}. A higher switching threshold triggers more frequent handover to the relay path and thus lowers the outage probability.

Taking the derivative of $P_{\text{avg}}(\gamma_{\text{th}})$ in (28) with respect to γ_{th} yields

$$\frac{\partial P_{\text{avg}}}{\partial \gamma_{\text{th}}} = (1-q) f_d(\gamma_{\text{th}})(P_s - P_d) > 0, \tag{32}$$

which indicates that $P_{\text{avg}}(\gamma_{\text{th}})$ is monotonically increasing with respect to γ_{th}; i.e., raising the switching threshold increases the average power consumption.

The above monotonicity analysis shows that the average power consumption and outage probability exhibit opposite monotonic trends with respect to γ_{th}. Therefore, the optimal solution to (30) is achieved when the outage probability constraint is tight:

$$\gamma_{\text{th}}^{*} = \min\big\{\gamma_{\text{th}} : P_{\text{out}}(\gamma_{\text{th}}) \le \epsilon_{\text{th}}\big\}. \tag{33}$$

The physical interpretation is clear: while satisfying the reliability constraint, the low-power direct link should be utilized for as long as possible, and the high-power satellite relay should be activated only when necessary.

When $\gamma_{\text{th}}^{*} = 0$, the system switches to the relay path only upon hard blockage, corresponding to a hard-blockage-triggered strategy. When $\gamma_{\text{th}}^{*} = \gamma_{\text{svc}}$, the system switches as soon as the direct-link SNR falls below the service threshold, corresponding to an SNR-threshold-triggered strategy. The specific operating mode is determined jointly by the scenario parameters $(q, m, \epsilon_{\text{th}})$.

Eq. (33) can be efficiently solved by a one-dimensional numerical search over $\gamma_{\text{th}} \in [0, \gamma_{\text{svc}}]$: the feasible region satisfying $P_{\text{out}}(\gamma_{\text{th}}) \le \epsilon_{\text{th}}$ is identified, and the minimum threshold in that region is selected as γ_{th}^{*}.

4.3 UAV Power Allocation Optimization

4.3.1 Problem Formulation

Given a limited total UAV transmit power budget P_{total}, the power allocation between the direct link and the satellite uplink is another critical factor affecting system performance. Let the allocation ratio be $\alpha \in (0, 1)$ such that

$$P_d = \alpha P_{\text{total}}, \quad P_s = (1 - \alpha) P_{\text{total}}. \tag{34}$$

The average SNR of each link scales linearly with its transmit power:

$$\bar{\gamma}_d(P_d) = \bar{\gamma}_{d,\text{nom}} \cdot \frac{P_d}{P_{d,\text{nom}}}, \quad \bar{\gamma}_u(P_s) = \bar{\gamma}_{u,\text{nom}} \cdot \frac{P_s}{P_{s,\text{nom}}}, \tag{35}$$

where $\bar{\gamma}_{d,\text{nom}}$ and $\bar{\gamma}_{u,\text{nom}}$ are the nominal average SNRs of the direct link and satellite uplink, respectively, under the reference power settings $P_{d,\text{nom}}$ and $P_{s,\text{nom}}$. The satellite downlink SNR $\bar{\gamma}_v$ is independent of α as P_v is fixed.

The objective is to minimize the system outage probability of the ideal SC benchmark under the total power constraint, which serves as a theoretical reference for the best achievable performance with power allocation:

$$\min_{\alpha} \; P_{\text{out,SC}}(\alpha) \quad \text{s.t.} \quad P_d + P_s = P_{\text{total}}, \quad 0 < \alpha < 1. \tag{36}$$

4.3.2 Solution via Golden-Section Search

From (17), $P_{\text{out,SC}}(\alpha) = P_{\text{out},d}(\alpha) \cdot P_{\text{out},r}(\alpha)$. Here, $P_{\text{out},d}(\alpha)$ decreases with α (more power to the direct link), while $P_{\text{out},r}(\alpha)$ increases with α (less power to the satellite uplink). The product is generally non-monotonic, and an optimal α^* exists that minimizes the outage probability.

Problem (36) is a one-dimensional constrained optimization that can be efficiently solved by golden-section search over $\alpha \in (0.05, 0.95)$, where the bounds avoid starving either link completely. For each candidate α, the average SNRs are updated via (35),

Table 1 System and Channel Parameters

Parameter	Direct Link	Satellite Relay
Carrier frequency (f_c)	842.5 MHz	1,995 MHz / 2,185 MHz
Transmit power	30 dBm	33 dBm
Antenna gain	2 dBi	2.5 dBi / 35 dBi
Bandwidth	200 kHz	20 kHz
Noise figure	5 dB	3 dB
Rician K-factor	10 dB	8 dB
Satellite altitude	—	35,786 km
Default elevation angle	—	30°

and the outage probability is computed using the expressions from Section 3. The search yields the optimal α^* that minimizes the system outage probability.

5 Numerical Results and Discussion

In this section, we provide simulation results to demonstrate the validity of the analytical expressions and investigate the effects of key system and channel parameters on the performance of the considered integrated satellite-aerial IoT network. Unless otherwise stated, the simulation parameters are summarized in Table 1. The direct link adopts a Rician fading channel with $K_d = 10$ dB, and the satellite uplink and downlink adopt SR fading channels with $K_s = 8$ dB and shadowing parameter $m = 5$. The service SNR threshold is set to $\gamma_{\text{svc}} = 5$ dB, and the target outage probability is $\epsilon_{\text{th}} = 10^{-2}$. The satellite elevation angle is set to 30° by default. Monte Carlo simulations are conducted with 10^5 independent channel realizations to ensure statistical accuracy.

5.1 Verification of Analytical Results

Figs. 2-4 compare the outage probability, ergodic capacity, and average BER of the three transmission paths (direct path, two-hop DF relay path, and ideal SC benchmark) as functions of the average SNR, respectively. The analytical curves are plotted using the expressions derived in Section 3, while the markers represent the Monte Carlo

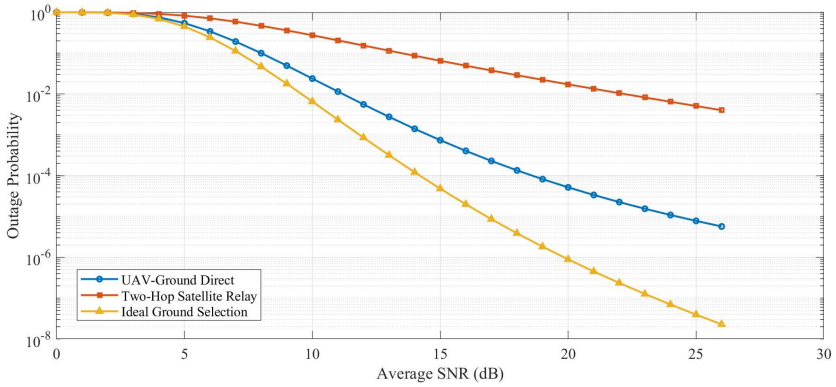


Fig. 2 Outage probability of the three transmission paths versus average SNR.

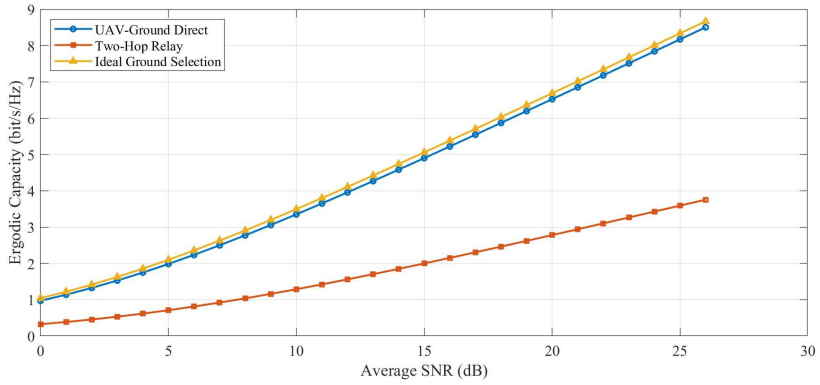


Fig. 3 Ergodic capacity of the three transmission paths versus average SNR.

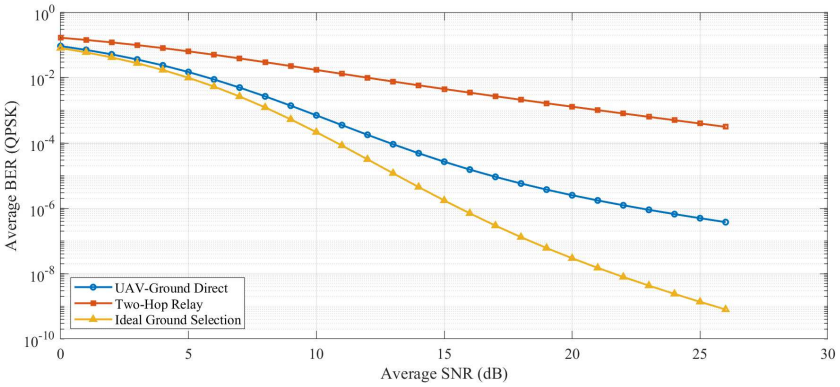


Fig. 4 Average BER of the three transmission paths versus average SNR.

simulation results. The asymptotic curves in the high-SNR regime are also included for comparison.

The analytical results closely match the Monte Carlo simulations across the entire SNR range, confirming the accuracy of the theoretical derivations. Furthermore, the asymptotic curves are in good agreement with the exact curves in the high-SNR region, validating the asymptotic analysis in Section 3.

Several observations are worth highlighting. Firstly, the direct path achieves the lowest outage probability, highest capacity, and lowest BER at moderate to high SNR. This is because the Rician K-factor of 10 dB implies a strong LoS component, which suppresses fading fluctuations and yields a near-Gaussian error performance. Secondly, the relay path achieves a slower performance improvement due to the bottleneck imposed by the weaker hop. Both satellite hops yield a diversity order of one, so the end-to-end diversity stays unity, and the weaker hop governs the overall coding gain. Thirdly, the half-duplex penalty further reduces the ergodic capacity of the relay path by a factor of two compared with a hypothetical full-duplex relay. Fourthly, the ideal SC benchmark provides the best performance among the three, benefiting from path diversity that yields diversity order two. However, this upper bound requires continuous full-CSI acquisition of both links and parallel signal reception chains, which is impractical for energy-constrained UAV IoT terminals.

5.2 Impact of Shadowing Parameter on Relay Performance

The shadowing parameter m characterizes the severity of LoS fluctuations for satellite links. When m is small (severe shadowing), the LoS power exhibits large fluctuations and the deep-fade probability increases substantially. As m grows, the LoS component becomes more stable, and the SR distribution gradually approaches a Rician distribution with the same K_s.

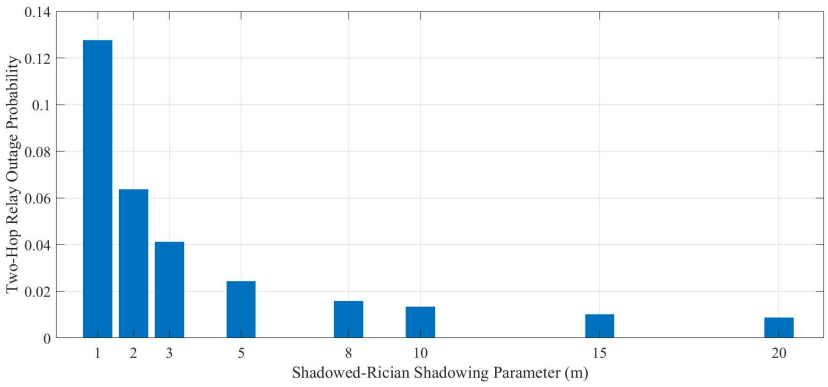


Fig. 5 Relay path outage probability versus shadowing parameter m.

Fig. 5 illustrates the impact of m on the outage probability of the two-hop relay path. As m increases from 1 to 20, the relay outage probability decreases from approximately 12.76% to 0.86%. The decline is most significant in the low-m region ($m \leq 5$), indicating that improving the stability of the satellite LoS component yields the highest reliability gain under severe shadowing conditions. For $m > 10$, the reduction flattens out, suggesting diminishing marginal returns under moderate to light shadowing. This saturation effect indicates that once the shadowing is sufficiently mild, further reducing shadowing fluctuations provides little additional benefit, and the system performance becomes limited by the multipath fading and the two-hop bottleneck instead. It is also observed that m mainly affects the coding gain rather than the diversity order of the relay path, which is consistent with the asymptotic analysis in Section 3.

5.3 Impact of Shadowing Parameter on Switching Performance

When the optimal switching threshold γ_{th}^{*} equals zero under the nominal configuration, switching is triggered exclusively by hard blockage rather than by SNR degradation. In this regime, the post-switch outage follows the identity $P_{\text{out,switch}} = q \cdot P_{\text{out},r} +$

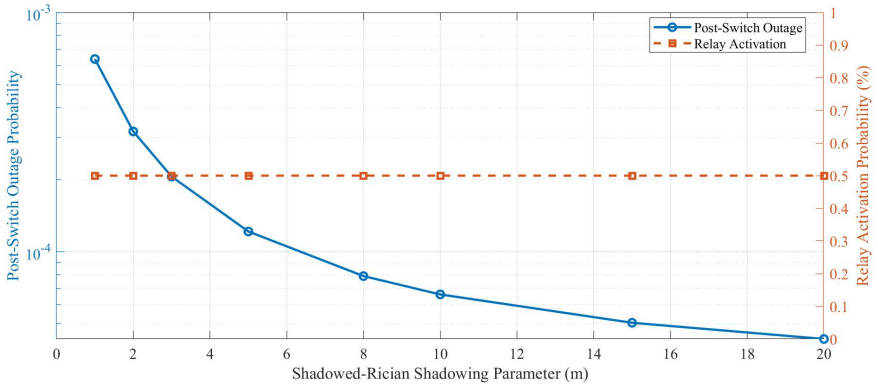


Fig. 6 Post-switch outage probability and relay activation probability versus shadowing parameter m under $q = 0.5\%$ hard blockage.

$(1-q) \cdot P_{\text{out},d}$. Since $P_{\text{out},d}$ is negligibly small under nominal conditions, the post-switch outage is approximately proportional to $q \cdot P_{\text{out},r}$, and thus inherits the same sensitivity to the shadowing parameter as the relay outage itself.

Fig. 6 presents the post-switch outage probability and relay activation probability as functions of m, with a fixed hard-blockage probability $q = 0.5\%$. As m increases from 1 to 20, the post-switch outage decreases from about 6.4×10^{-4} to about 4.3×10^{-5}, a one-order-of-magnitude improvement, with the steepest drop occurring in the low-m region ($m \leq 5$). In contrast, the relay activation probability remains nearly constant (around 0.5%) across the entire m range. This indicates that the switching frequency is primarily determined by the hard-blockage probability q and is almost unaffected by shadowing conditions. Consequently, improving satellite link stability directly enhances the post-switch reliability without incurring additional power overhead from more frequent relay activation—a highly desirable property from an energy-efficiency perspective.

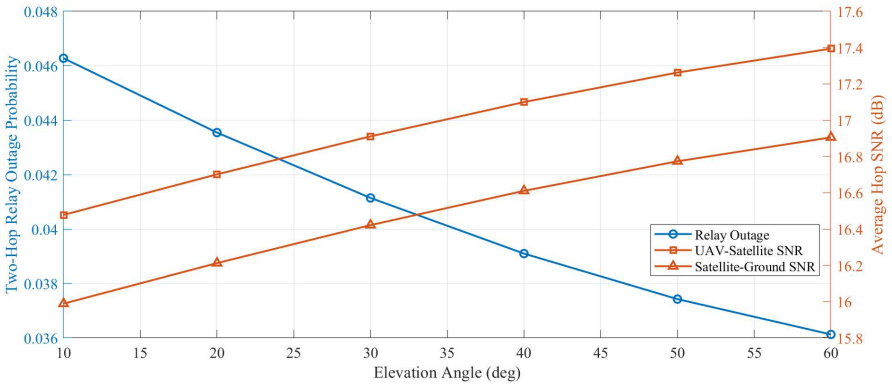


Fig. 7 Relay outage probability and hop average SNR versus satellite elevation angle.

5.4 Impact of Satellite Elevation Angle

The satellite elevation angle θ affects the slant range between the UAV and the satellite, and thus the average received SNR of the satellite uplink and downlink. Higher elevation angles yield shorter propagation distances and higher link SNR, whereas low elevation angles correspond to longer path lengths and greater propagation loss. In the present model, the shadowing parameters are treated as invariant with elevation, so the effect of elevation is captured mainly through the geometric path-loss term.

Fig. 7 shows the relay path outage probability and the corresponding average SNR as functions of θ. As the elevation angle increases from 10° to 60°, the average SNR of the satellite uplink increases from approximately 16.5 dB to 17.4 dB, and the relay outage probability decreases accordingly. In the low-elevation region ($\theta \leq 20^\circ$), the longer path length translates into lower received SNR and thus poorer relay reliability. In the high-elevation region ($\theta \geq 40^\circ$), the shorter slant distance yields higher link SNR, and the relay path can provide more reliable backup transmission. This result provides guidance for constellation selection and beam planning when deploying satellite IoT systems in remote areas.

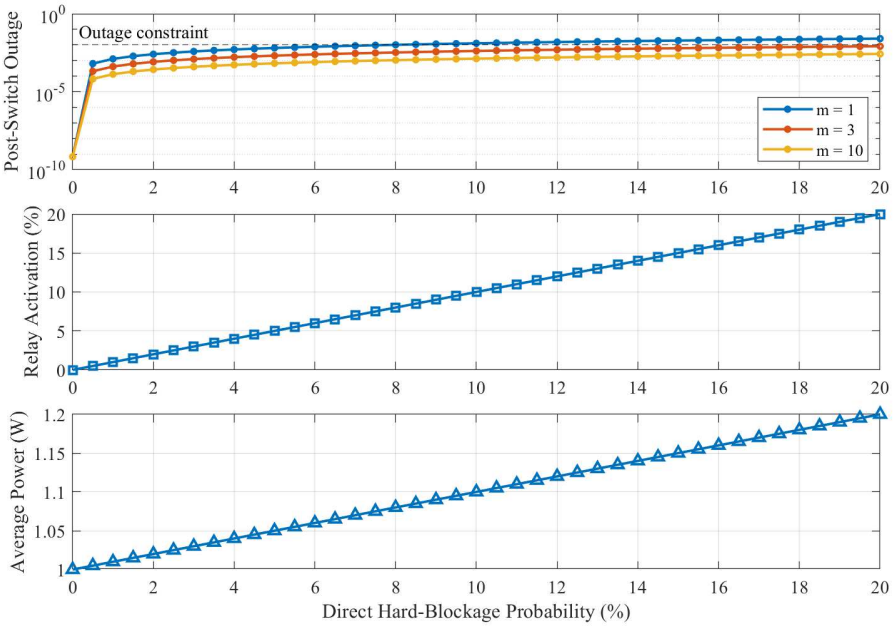


Fig. 8 System outage probability versus direct-link hard-blockage probability q under different shadowing conditions.

5.5 Impact of Direct-Link Hard-Blockage Probability

The hard-blockage probability q is a key parameter that determines the frequency of relay activation. For a direct-link-only system, the outage probability is $q + (1 - q)P_{\text{out},d}$, which increases nearly linearly with q when the fading-induced outage $P_{\text{out},d}$ is negligible. After introducing a satellite relay backup, the system outage becomes $q \cdot P_{\text{out},r} + (1-q)P_{\text{out},d}$. The satellite relay serves as a redundancy layer to handle hard-blockage events. When the direct link is blocked, the system switches to the satellite path, and the overall outage equals the product of the blockage probability and the relay outage probability. This multiplicative reduction is the fundamental mechanism behind the effectiveness of the primary-backup switching strategy.

Fig. 8 investigates the sensitivity of the system to q. For the system using only the direct path, the outage probability increases nearly linearly with q in the range $10^{-3} \leq q \leq 10^{-1}$. After introducing the satellite relay backup, the outage reduction

Table 2 Primary/Backup Switching Results for Three Scenarios

Scenario	m	q (%)	ϵ_{th} (%)	$P_{\text{out,direct}}$ (%)	$P_{\text{out,switch}}$ (%)	**Reduction** (%)
Forest Fire Emergency	1	0.5	0.1	0.5000	0.06379	87.24
Glacier/Ocean Monitoring	10	1.0	5.0	1.0000	0.01324	98.68
Urban Edge Inspection	5	2.0	1.0	2.0000	0.04852	97.57

is most dramatic when the relay path has high reliability (large m): for $m = 20$, the outage drops by more than an order of magnitude at $q = 10^{-2}$. It is also observed that the benefit of increasing m is more pronounced at larger q. This is because when blockages are rare (small q), the direct link handles most transmissions and the relay quality matters less. When blockages are frequent (large q), the relay is called upon more often, and its reliability has a larger impact on the overall system performance.

5.6 Switching Performance under Three Monitoring Scenarios

Table 2 summarizes the primary/backup switching results for three representative environmental monitoring scenarios: forest fire emergency, glacier/ocean monitoring, and urban edge inspection. The direct-link-only outage probability $P_{\text{out,direct}}$ equals the hard-blockage probability q, as the direct link enjoys a high Rician K-factor and its fading-induced outage is negligible under nominal SNR conditions. The switching strategy, with the optimal threshold γ_{th}^* determined by (33), significantly reduces the outage probability in all three cases while satisfying the respective constraint ϵ_{th}.

In all three scenarios, the optimal switching threshold γ_{th}^* equals zero, meaning that the system switches to the relay path only upon hard blockage of the direct link and that SNR-triggered handover is not activated. This is because the direct link operates with a large link margin (average SNR far above the service threshold), so that the fading-induced outage probability of the direct link is negligible compared with the hard-blockage probability q. Consequently, the outage reduction achieved by

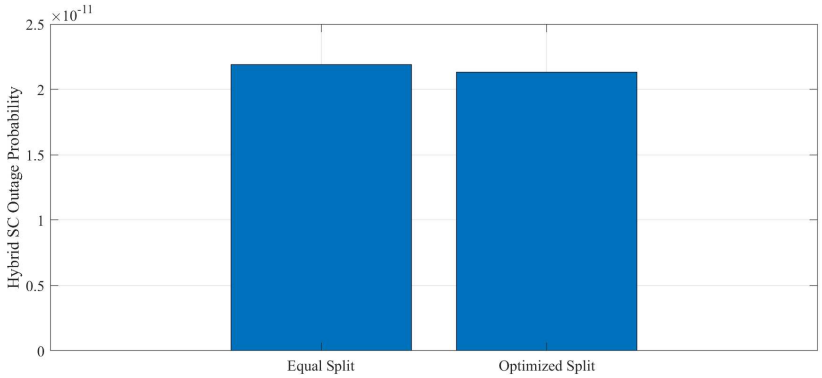


Fig. 9 Outage probability under equal-power and optimized power allocation.

the proposed strategy is primarily due to the availability of a satellite backup, rather than from SNR-based threshold optimization.

In the forest fire emergency scenario ($m = 1$, $q = 0.5\%$, $\epsilon_{\text{th}} = 0.1\%$), severe shadowing limits the reliability of the satellite relay, resulting in an 87.24% outage reduction, which is the smallest among the three scenarios. In the glacier/ocean monitoring scenario ($m = 10$, $q = 1.0\%$, $\epsilon_{\text{th}} = 5.0\%$), the relay path is highly reliable and the outage drops by 98.68%, the largest reduction. The urban edge inspection scenario ($m = 5$, $q = 2.0\%$, $\epsilon_{\text{th}} = 1.0\%$) achieves a 97.57% reduction, confirming that the proposed switching strategy is effective even under frequent blockages. The SNR-threshold regime becomes relevant only when the direct-link margin is substantially reduced, e.g., at longer communication ranges or lower transmit power.

5.7 Power Allocation Optimization

Fig. 9 compares the outage probability of the hybrid system under equal-power splitting ($\alpha = 0.5$) and the optimized allocation obtained via golden-section search. Under the nominal power settings ($P_d = 30$ dBm, $P_s = 33$ dBm), both schemes achieve extremely low outage probabilities, and the optimized allocation yields a marginal improvement of about 2%–3%. The small gain is attributed to the fact that at such

high nominal powers, both links have ample SNR margins, leaving little room for further improvement.

Nevertheless, the following trends are observed. In the low total power region, the satellite uplink is the bottleneck, and the system tends to allocate more power to the uplink ($\alpha^* < 0.5$) to balance the outage probabilities of the two paths. As total power increases and the uplink SNR surpasses the downlink SNR, further boosting P_s yields diminishing returns, and α^* shifts toward the direct link. The gain brought by optimal power allocation is modest at the nominal operating point, approximately 2%–3%. This gain stays less than one order of magnitude over the investigated power range, and the maximum gain appears at a transmit power much lower than the nominal UAV operating level. This confirms that power allocation optimization provides the largest benefit in severely power-limited scenarios, while its impact is limited under typical operating conditions.

6 Conclusions

In this paper, we have investigated the performance of a UAV-based integrated satellite-aerial IoT system with a primary-backup link switching strategy over heterogeneous Rician and SR fading channels. By considering the practical hard-blockage effect of the direct link, a realistic hybrid system model was developed for remote environmental monitoring scenarios. Based on the derived statistical characteristics of both links, analytical expressions for the outage probability, ergodic capacity, and average BER were obtained for the direct path, the two-hop DF relay path, and the switching system, respectively. To gain further insight, asymptotic analysis at high SNR was performed, showing that both individual paths achieve diversity order one while the selection combining benchmark achieves diversity order two.

By exploiting the opposite monotonicity of outage probability and average transmit power versus the switching threshold, the optimal threshold is found at the outage constraint boundary. This property reduces the constrained power-minimization problem to a one-dimensional root-finding task. The parameter regime requiring SNR-triggered switching beyond pure blockage triggering is also characterized. The optimal threshold is strictly positive only when the fading-induced outage of the direct link is comparable to the hard-blockage probability. Under nominal high-margin configurations, the threshold degenerates to zero, and the strategy is triggered merely by hard blockage. Finally, a golden-section-search-based power allocation scheme was adopted to further improve the system performance. Monte Carlo simulation results were provided to corroborate the analytical results and to demonstrate the impacts of key parameters, including the shadowing parameter, blockage probability, elevation angle, and power allocation ratio.

It should be noted that several simplifications are adopted in this work. Hard blockage is modeled as an independent and identically distributed (i.i.d.) process. This blockage follows a Bernoulli process with fixed probability q. Under temporally correlated blockage, the reported gains serve as an upper bound. In addition, perfect CSI of the direct link is assumed, and only transmit power is considered within the power model. Extensions to imperfect CSI, temporally correlated blockage, and a more comprehensive power model constitute interesting directions for future research.

References

[1] Tropea, M.: State-of-the-art in satellite communication networks. Electronics **11**(9), 1368 (2022) https://doi.org/10.3390/electronics11091368

[2] Gao, Q., Jia, M., Guo, Q., Gu, X., Hanzo, L.: Jointly optimized beamforming and power allocation for full-duplex cell-free NOMA in space-ground integrated networks. IEEE Trans. Commun. **71**(5), 2816–2830 (2023) https://doi.org/10.

1109/TCOMM.2023.3251342

[3] Zeng, Y., Wu, Q., Zhang, R.: Accessing from the sky: A tutorial on UAV communications for 5G and beyond. Proc. IEEE **107**(12), 2327–2375 (2019) https://doi.org/10.1109/JPROC.2019.2952892

[4] Li, H., Mao, K., Zhu, Q., Ye, X., Chen, X., Li, H., Briso-Rodriguez, C., Zhong, W.: Measurement-based vegetation penetration loss model for UAV-to-ground communications. In: 2024 IEEE 100th Vehicular Technology Conference (VTC2024-Fall), pp. 1–5 (2024). IEEE

[5] Abdi, A., Lau, W.C., Alouini, M.-S., Kaveh, M.: A new simple model for land mobile satellite channels: first- and second-order statistics. IEEE Trans. Wirel. Commun. **2**(3), 519–528 (2003) https://doi.org/10.1109/TWC.2003.811182

[6] Bhatnagar, M.R.: Performance evaluation of decode-and-forward satellite relaying. IEEE Trans. Veh. Technol. **64**(10), 4827–4833 (2015) https://doi.org/10.1109/TVT.2014.2373389

[7] Jung, D.-H., Ryu, J.-G., Byun, W.-J., Choi, J.: Performance analysis of satellite communication system under the Shadowed-Rician fading: A stochastic geometry approach. IEEE Trans. Commun. **70**(4), 2707–2721 (2022) https://doi.org/10.1109/TCOMM.2022.3142290

[8] Zhang, C., Li, K., Xu, C., Yang, L.-L., Hanzo, L.: Space-air-ground-integrated networks: The BER vs. residual delay and Doppler analysis. IEEE Open J. Veh. Technol. **7**, 1351–1367 (2026) https://doi.org/10.1109/OJVT.2026.3688310

[9] Hu, X., Lin, B., Wang, P., Lu, X.: LEO satellite and UAV-assisted maritime internet of things: Modeling and performance analysis for data acquisition. Future Internet **18**(1), 24 (2026) https://doi.org/10.3390/fi18010024

[10] Celebi, B.A., Akyol, O.F., Basaran, S.T., Hokelek, I., Gorcin, A.: On outage analysis of OTFS based LEO-satellite systems with HAPS relaying. In: 2024 IEEE Future Networks World Forum (FNWF), pp. 260–265 (2024). IEEE

[11] Sharma, P.K., Upadhyay, P.K., Da Costa, D.B., Bithas, P.S., Kanatas, A.G.: Performance analysis of overlay spectrum sharing in hybrid satellite-terrestrial systems with secondary network selection. IEEE Trans. Wirel. Commun. **16**(10), 6586–6601 (2017) https://doi.org/10.1109/TWC.2017.2725950

[12] Verma, A., Sharma, P.K., Mahapatro, J.: Outage analysis of space–air–ground integrated networks powered by battery-aided SWIPT. IEEE J. Miniaturization Air Space Syst. **7**(1), 99–115 (2026) https://doi.org/10.1109/JMASS.2025.3644243

[13] Srivastava, P., Sai Kiran, M.P.R., Singh, A.K.: Outage analysis in directional NTN links with UAV platform instabilities. IEEE Trans. Veh. Technol. **75**(6), 9893–9908 (2026) https://doi.org/10.1109/TVT.2025.3633865

[14] Guo, K., An, K.: On the performance of RIS-assisted integrated satellite-UAV-terrestrial networks with hardware impairments and interference. IEEE Wirel. Commun. Lett. **11**(1), 131–135 (2022) https://doi.org/10.1109/LWC.2021.3122189

[15] Senadhira, N., Durrani, S., Guo, J., Yang, N., Zhou, X.: Design and performance analysis of UAV-assisted maritime-LEO satellite communication networks. IEEE Open J. Commun. Soc. **6**, 4667–4688 (2025) https://doi.org/10.1109/OJCOMS.2025.3571757

[16] Wang, C., Yang, X., Du, Q., Wang, J.: Outage performance of satellite-UAV network framework based on NOMA. In: 2021 IEEE 5th International Conference

on Cryptography, Security and Privacy (CSP), pp. 171–175 (2021). IEEE

[17] Wang, T., Badiu, M.-A., Chen, G., Coon, J.P.: Outage probability analysis of RIS-assisted wireless networks with Von Mises phase errors. IEEE Wirel. Commun. Lett. **10**(12), 2737–2741 (2021) https://doi.org/10.1109/LWC.2021.3113830

[18] Xue, G., Yang, M., Guo, Q., Yuan, S.: Performance of spectrum sharing in hybrid satellite terrestrial network with opportunistic relay selection. Wirel. Commun. Mob. Comput. **2022**(1), 2673024 (2022) https://doi.org/10.1155/2022/2673024

[19] Wu, Z., Wang, Q.: Trajectory optimization and power allocation for cell-free satellite-UAV internet of things. IEEE Access **11**, 203–213 (2023) https://doi.org/10.1109/ACCESS.2022.3232945

[20] Lin, H., Zhang, C., Huang, Y., Zhao, R., Yang, L.: Downlink outage analysis of integrated satellite-terrestrial relay network with relay selection and outdated CSI. In: 2021 IEEE 93rd Vehicular Technology Conference (VTC2021-Spring), pp. 1–5 (2021). IEEE

Statements and Declarations

Competing interests

The authors declare that they have no competing interests.

Ethics approval and consent to participate

Not applicable.

Consent for publication

Not applicable.

Data availability

The datasets generated and analysed during the current study are available from the corresponding author on reasonable request.

Materials availability

Not applicable.

Code availability

The simulation code used in this work is available from the corresponding author upon reasonable request.